Broadband Light-matter Interaction Due to Resonance Cavities in Graded Photonic Super-crystals

SAFAA HASSAN,¹ OLIVER SALE,¹ KHADIJAH ALNASSER,¹ NOAH HURLEY,¹ HUALIANG ZHANG,² USHA PHILIPOSE,¹ AND YUANKUN LIN^{1, 3, *}

¹Department of Physics, Univ. of North Texas, Denton, TX 76203, USA

Abstract: In this paper, we report the formation of resonance cavities within graded photonic super-crystals (GPSCs) with unit cells formed via a near-uniform central region with eight side graded regions. The graded regions in the GPSCs have several photonic band gaps, whereas the uniform region has one photonic band gap. The different locations of the photonic band gaps form a central cavity and eight surrounding side cavities with more cavities at the boundary of the corresponding uniform and graded regions. The quality-factor of the cavities in the boundary regions has been calculated to be as high as 5.8×10^5 . The central and side cavities have a relatively low-quality factor. Broadband light-matter interaction has been observed in the simulation of transmission through the GPSC. When the thickness of the GPSC is out of resonance with the central cavity mode, the dip in the transmission through the GPSC is shallow and narrow. When the thickness of the GPSC is in-resonance with the central cavity mode, a wide and deep transmission dip is observed in the wavelength range in the photonic band gap of the graded regions. This indicated that the coupling of in-plane resonance in the central region with the Fabry-Perot resonance in the GPSC is occurring.

© 2019 Optical Society of America

1. Introduction

Photonic crystals (PhCs) are periodic structures that have a lattice constant comparable to the desired operation wavelength [1]. PhCs have been used for the manipulation and control of light. Usually, desired defects are needed to engineer the function of the PhC. For example, point defects in PhCs have been used as resonance cavities for nano-lasers with low lasing thresholds which can be further developed as single photon sources [2-8]. Line defects in PhCs have been used as waveguides for future optoelectronic device integration [9]. Other functional defects such as ring resonators and coupled cavities have been used for beam coupling and channel drop in optical chips [10-12].

Recently hetero-structure PhCs have been used for cavity laser devices [13-18]. The 2D PhC hetero-structure can be fabricated via adjusting the lattice constant, the lattice symmetry, or the filling fraction (air hole radius). These micro-resonator devices can have a high quality-factor (Q-factor) and a small dimension suitable for micro- and nano-photonics. Very recently, graded photonic super-crystals (GPSCs) have been studied for their novel optical properties: specifically, the high light extraction efficiency when the cathode of organic light emitting diodes is patterned with the GPSC, and the simultaneous formation of GPSC and desired defects [19-23]. The GPSC was named for the gradient size of the dielectric post or air hole in a unit cell and a large size of super-cell. Moreover, the GPSC can have graded lattice clusters arranged in square, five-fold, or hexagonal symmetries [19-23]. When a high number of graded lattice clusters are formed in ring-type geometry in a GPSC, a hetero-structure GPSC can be

²Department of Electrical & Computer Engineering, Univ. of Massachusetts Lowell, Lowell, MA 01854, USA

³Department of Electrical Engineering, Univ. of North Texas, Denton, TX 76203, USA. *yuankun.lin@unt.edu

obtained via photonic band gap engineering. The first cavity in a 2D PhC was experimentally demonstrated in 1999 [24] and many types of cavities with high Q-factor have been reported since 1999 [13-18]. Traditionally, a single cavity was fabricated in 2D PhC in a small area using slow E-beam lithography. However, via holographic lithography, a high number of cavities can be fabricated simultaneously over a large area template in the 2D PhC in a single exposure.

An octagonal GPSC, comprised of a central near-uniform (very small variation of cylinder size) region surrounded by 8 graded lattice clusters (8 graded regions), can form resonances that are able to couple simultaneously in two configurations: octagonal and square. These octagonal and square resonances have different ring lengths which have potential use as side and link rings, respectively, in topological photonics [25, 26]. This feature was not observed in previously reported GPSCs [19-23] or in traditional PhC-based resonators with one periodicity.

In this paper, we simulated the photonic band gaps in the octagonal GPSC and observed three types of resonance cavities where the boundary cavity has a high quality factor. The transmission through the octagonal GPSC is also simulated. Broadband transmission dips are located at the photonic band gap of the graded regions, indicating the coupling of the cavity resonance in the central regions with the quasi bound state in the continuum (BIC) [27] of the GPSC, and a potential application in broadband detectors [28-29].

2. Photonic Band Structures in Graded Photonic Super-Crystal for the Formation of Cavity

GSPCs can be formed via two sets of graded basis. As seen in Fig. 1(a), the solid purple square indicates a near-uniform region and the solid red square indicates the graded region. Along the dashed red (blue) lines, the rod basis on the lattice increases (decreases) in the direction of the solid red square. When these graded regions create a five-fold, hexagonal or rectangular symmetry, the overall symmetry is no longer square and the resultant photonics band structures are difficult to calculate. The graded region (near-uniform region) in the solid red (purple) square in Fig. 1(a) has a square symmetry when the overall symmetry in the GPSC is square. Thus, it is easy to simulate the photonic band structure in the graded and near-uniform regions, respectively.

Hence, to attain a simulated unit cell with overall square symmetry, we generated an interference pattern from two sets of interfering beams (i.e. four inner and four outer beams) [26]. The four outer beams were arranged in cone format in square symmetry with a large interfering angle θ_1 . Their wave-vectors can be written $k(\sin(\theta_1)\cos(45),\sin(\theta_1)\sin(45),\cos(\theta_1)),$ $k(\sin(\theta_1)\cos(135),$ $\sin(\theta_1)\sin(135),\cos(\theta_1)$, $k(\sin(\theta_1)\cos(225), \sin(\theta_1)\sin(225), \cos(\theta_1)), \text{ and } k(\sin(\theta_1)\cos(315), \sin(\theta_1)\sin(315), \cos(\theta_1)).$ The four inner beams were arranged in a similar geometry with a small interfering angle θ_2 and wave-vectors: $k(\sin(\theta_2)\cos(45),$ $\sin(\theta_2)\sin(45)$, $\cos(\theta_2)$), $k(\sin(\theta_2)\cos(135),$ $\sin(\theta_2)\sin(135)$, $\cos(\theta_2)$), $k(\sin(\theta_2)\cos(225)$, $\sin(\theta_2)\sin(225)$, $\cos(\theta_2)$), and $k(\sin(\theta_2)\cos(315)$, $\sin(\theta_2)\sin(315), \cos(\theta_2)$.

Figure. 1(a) shows the result of an eight-beam (four inner and four outer beams) interference pattern (square lattice in square symmetry) when exposure wavelength=532 nm, θ_1 =20.6 degrees and θ_2 =1.8 degrees in above equations. The iso-intensity, I(r), of the interference pattern is used as an input for the generation of binary dielectric/air structures for the simulation of photonic band gaps in the GPSC. The binary dielectric/air structures are obtained by comparing I(r) with a threshold intensity I_{th}, via the step functions: $\epsilon(r) = 1$ (for air) when I<I_{th}, and $\epsilon(r) = 12$ (for a high refractive index material) when I>I_{th}. The resulting dielectric/air structure is shown via the a-insert (Fig. 1).

Photonic band structures for the TE modes in the 2D GPSC were computed using the MIT Photonic Bands (MPB) software package [30] via the Simpetus Electromagnetic Simulation Platform via Amazon Web Services. For the 6x6 cell of rods in Fig. 1(a), we increased the size of the lattice by six, and then added all of the rods in the MPB program. Parallel computations in a 36-core virtual machine were used in the calculation of the simulated photonic band

structures. The computation took approximately 30 minutes to complete. The results for the near-uniform and graded region are shown in Fig. 1(b) and 1(c), respectively.

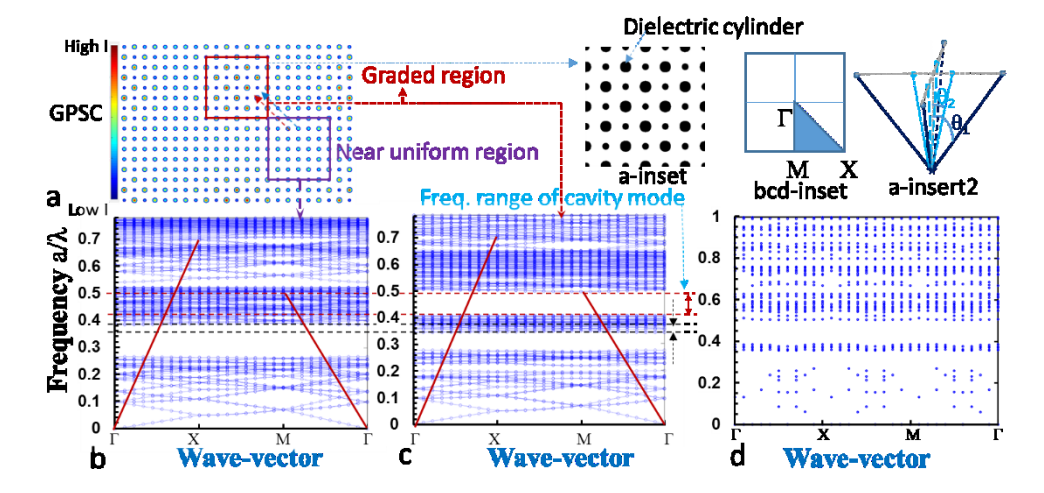


Figure 1. (a) Interference pattern as an input for the simulation of photonic band structure of the GPSCs; (b) Simulated photonic band gap for TE mode for the near-uniform region in purple squares in (a) using MIT MPB program; (c) Simulated photonic band gaps for TE mode for the graded region in red squares in (a) using MIT MPB program. (d) Simulated photonic band gaps for TE mode for the graded region in red squares in (a) in 3D GPSC using the MIT MEEP program. A thickness of one lattice constant was used for the GPSC. a-insert shows a cross-section of binary dielectric distribution from the graded region in (a). bcd-insert shows the high-symmetry points in the Brillouin zone that are labeled in the x-axis in (b-c). a-insert2 shows the eight beam configuration and interfering angles.

For the near-uniform region in Fig. 1(a), there is one photonic band gap (Fig. 1(b)). While for the graded region in Fig. 1(a), there are two photonic band gaps (Fig. 1(c)). To aid in comparison of these band structures in Fig. 1(b) and 1(c), the black arrows (Fig. 1(c)) indicate the frequency range for the allowed (forbidden) modes in the graded region in the graded (near-uniform) region (Fig. 1(a)); The red arrows (Fig. 1(c)) indicate the frequency range for the allowed (forbidden) modes in the uniform (graded) region (Fig. 1(a)). Fig. 1(d) shows the photonic band structures for the TE modes in the 3D GPSC where the graded region in Fig. 1(a) and a thickness of one lattice constant were used. The simulation was performed using the MIT MEEP program. Although the lower bands were not fully computed in Fig. 1(d), two band gaps appeared at $a/\lambda=0.28\sim0.35$ and $0.4\sim0.5$, the same locations as these in Fig. 3(c).

Figure 2(a) shows the interference pattern of a unit cell with eight graded regions in a ring-type structure around the central uniform region. Since the uniform region is surrounded by many graded regions in a ring-type structure, then cavity modes exist due to dislocation between the photonic band gaps in the graded regions and the near-uniform region. The fabricated sample has a unit cell size of $24a \times 24a$ [26] (a is the lattice constant as shown in Fig. 2(a)), while the simulated interference pattern has a unit cell size of $18a \times 18a$ as the parallel computation was unable to finish the simulation of the photonic band structure for the GPSC for larger unit cell sizes. The pattern in Fig. 2(a) was generated via interference of 8 beams whose azimuthal angles are the same as those in experimental setup [26]. The wave-vectors of one set of beams in cone geometry are described by $k(\sin(\theta_1)\cos(Out_{1-4}), \sin(\theta_1)\sin(Out_{1-4}), \cos(\theta_1))$, where the outer beam azimuthal angle Out_{1-4} is 45, 135, 225, and 315 degrees for each of the 4 beams, respectively. The wave-vectors for the other set of beams in cone geometry are described by $k(\sin(\theta_3)\cos(Inner_{5-12}), \sin(\theta_3)\sin(Inner_{5-12}), \cos(\theta_3))$, where the inner beam

azimuthal angle Inner₅₋₁₂ is α , $90-\alpha$, $90+\alpha$, $180-\alpha$, $180+\alpha$, $270-\alpha$, $270+\alpha$, and $360-\alpha$ for each of the 8 beams (α =26.57 degrees), respectively.

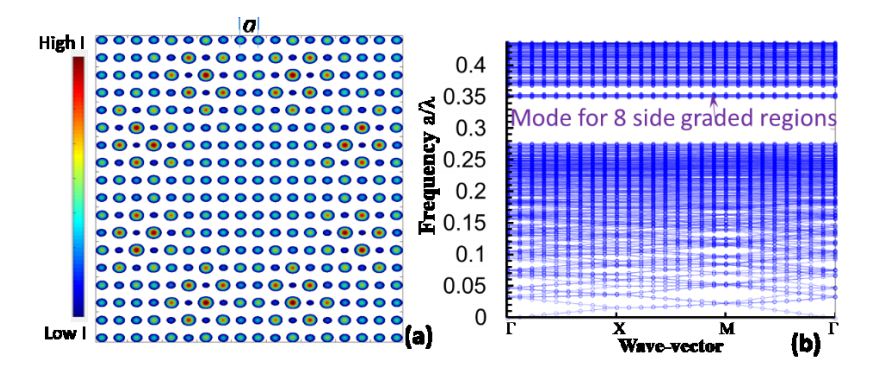


Figure 2. (a) Interference pattern for the 4-fold (8 graded regions) GPSC with a unit cell size of $18a \times 18a$. (b) Simulated photonic band structure of the GPSC with the unit super-cell in (a) by setting the threshold intensity I_{th} =26% I_{max} .

Fig. 2(b) shows the simulated photonic band structure in the GPSC with a unit super-cell size of $18a\times18a$ (Fig. 2(a)). The GPSC was generated with a threshold intensity of I_{th} =26% I_{max} . A mode appears at a frequency of a/λ =0.35. From direct comparison of Fig. 2(b) with the results in Fig. 1, this mode is due to the cavity in the eight graded regions.

3. E-field Distribution in Cavities in GPSC

A simulation of the electric field (E-field) intensity distributions was performed for a GPSC with a thickness of 2a and a unit cell size of $24a\times24a$, the same size as the experimental sample [26]. Fig. 3(a) shows the E-field intensity at the wavelength of $a/\lambda=0.35$. The binary GPSC was obtained from the interference pattern with a threshold intensity of $I_{th}=26\%I_{max}$ for Fig. 3(a). The E-field intensity and Q-factor for the cavities were calculated using the harmonic inversion function [31] included in the MIT MEEP software and computed via Amazon Web Services [32-33]. The computation took approximately one hour for one run using MEEP.

As shown in Fig. 3(a), the electric field is confined in the eight graded regions, confirming the prediction for the mode based on the photonic band structure simulation in Fig. 2(b) and Fig. 1. By creating a ring-type structure via eight graded regions (Fig. 2(a)), a cavity is formed in the central near-uniform region. A simulation of E-field distributions at the wavelength of a/λ =0.42 is shown in Fig. 3(b) for the GPSC obtained from the binary interference pattern with a threshold intensity $I_{th}=26\%I_{max}$. This shows that the electric field is confined in the central region in the wavelength region as predicted by Fig. 1(c). The resonance frequencies for the side graded regions and the central near-uniform region are dependent on the threshold intensity used for the binary GPSC. The higher the threshold intensity for obtaining a binary GPSC, the higher the resonance frequencies in the cavity in the graded and central regions in Fig. 3(a) and 3(b), respectively. Because of the large area of the near-uniform region, many resonance modes occur within the photonic band gap of the graded region. For example, Fig. 3(b) shows one mode oscillating in the vertical direction and one mode in a square shape around the boundary of the graded regions and the central region. Moreover, by tuning the threshold intensity to $25\%I_{max}$, fewer modes are observed at the given frequency $a/\lambda=0.42$ as shown in Fig. 3(c) where the oscillation is horizontal.

The E-field distribution and Q-factors for the side and central modes have been computed across a wide range of frequencies. The resonance modes in eight side cavities exist only in a very narrow frequency range. Q-factors were obtained for the frequencies of a/λ of 0.35 and 0.36 for the insert in Fig.3(a) within the frequency range indicated by the dash blue lines in Fig. 1(b-c) and dark arrows in Fig. 1(c). The Q-factor can only go up to 1688. For the central cavity,

we were able to observe the resonance modes in a wide frequency range. Q-factors was obtained for the frequencies of a/λ over a range from 0.41 to 0.48, within the frequency range indicated by the dash red lines in Fig. 1(b-c) and red arrows in Fig. 1(c). The Q-factor can only go up to 13840. The dark and red arrows in Fig. 1(c) indicates the allowed mode frequencies in either graded regions or near-uniform region. Thus, we concluded that the existence of cavity resonances in Fig.3(a-c) are due to the band gap effect.

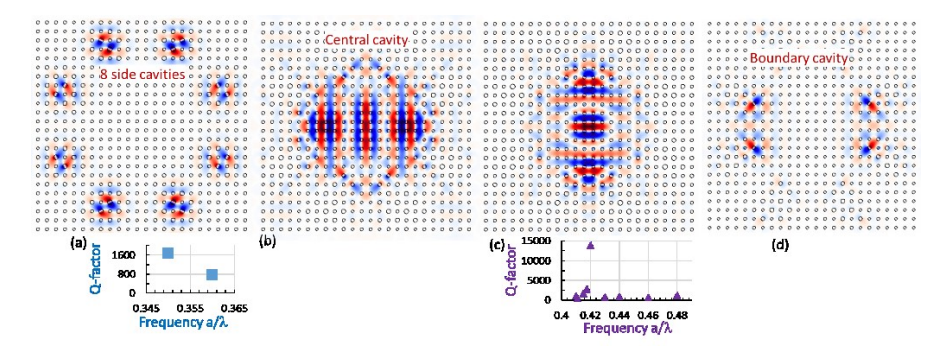


Figure 3. (a-b) Simulated electric field distributions in eight side cavities (a/ λ =0.35) and central cavity (a/ λ =0.42), respectively, in the GPSC with a unit cell size of 24a×24a obtained from the interference pattern with a threshold intensity I_{th} =26% I_{max} . (c) Simulated electric field distributions in the central cavity at a frequency a/ λ of 0.42 and a threshold intensity I_{th} =25% I_{max} . (d) Simulated electric field distributions for the boundary cavity at a frequency a/ λ of 0.41 and a threshold intensity I_{th} =28% I_{max} . The insets in (a) and (c) show Q-factors for side cavities and central cavity, respectively.

Given I_{th} =28% I_{max} and a/λ =0.410, only boundary cavities between the graded and uniform regions are observed (Fig. 3(d)). Q-factors for the boundary cavity modes have been calculated as high as 5.8×10^5 at the frequency a/λ =0.409 and I_{th} =28% I_{max} . The Q-factors for the side and central modes are much lower than these boundary modes. Another mechanism, such as the topological effect [25-26] instead of a band gap effect, is needed to explain this phenomenon. Hexagonal lattice configuration is usually used for topological photonics study. It can be further studies if a super-cell of hexagonal clusters of the square lattice can be programmed in MEEP or MPB.

4. On-resonance and Off-resonance Transmission through GPSC

Because photonic band gaps in Fig. 1 and Fig. 2 occur at frequencies below $a/\lambda=0.5$, the cavity laser can, in general, operate with modes below the light line (or light cone) as indicated by solid red lines in Fig. 1(b-c) [34-35]. Since the boundary mode in Fig. 3(d) is almost confined within the unit cell, the boundary cavity can be used for a lasing cavity. However, the central resonant modes in Fig. 3(b) and 3(c) extend over multiple unit cells, and, thus, will radiate (leak) in out-of-plane direction (z-direction) although they are below the light line. This is the reason why the Q-factors for most of these modes are below 1000 as shown in the insert in Fig. 3(c). Due to the leaking modes, the transmission in z-direction through the GPSC can be high even the light wavelength is within the band gap. However, a low transmission in the z-direction is expected if the light within the band gap is coupled with out-of-plane resonance modes such as the quasi BIC [27] and Fabry-Perot (F-P) resonance as studied below.

The transmission of light through the GPSC slab was simulated using MEEP. A unit cell size of $18a \times 18a$, instead of $24a \times 24a$, was used due to the limit of computation power. The light source was incident into the GPSC in the normal direction. We simulated the transmission for GPSC with periods 350, 500 and 765nm. In one group simulation, the thicknesses D (or depth) of the GPSC was selected by meeting the F-P resonance through solving the coupled equations: $a/\lambda=0.42$ (Fig. 3(b)), $\lambda=n\times D$ where n is the refractive index (the optical path length equals one

wavelength at the frequency a/λ =0.42). Therefore, D=242, 345 and 527 nm were used for the GPSC with periods of 350, 500 and 765 nm, respectively. The blue circles in Fig. 4(a) show the transmission through the GPSC with a=765 nm and D=527 nm. There is a broadband transmission dip between 1536 and 1842 nm measured at 20% transmission corresponding to a/λ of 0.498 and 0.415. The values of a/λ , where λ is the wavelength located at 20% of transmission dip, are plotted in Fig. 4(b) for the GPSC for periods of 350, 500 and 765 nm and with D=242, 345 and 527 nm, respectively. The top and bottom frequency edges in Fig. 4(b) correspond to the photonic band gap edges in Fig. 1(c) for the graded regions, indicating a strong coupling of in-plane resonance in the central region with the out-of-plane F-P resonance (quasi BIC) [27].

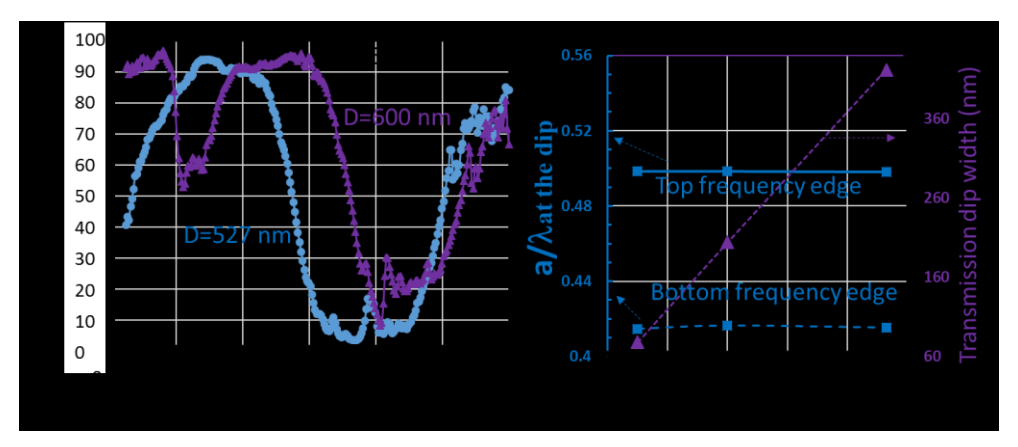


Figure 4. (a) Transmission of normal incident light through the GPSC with a unit cell size of $18a \times 18a$ (a=765 nm) for slab thicknesses of 527 nm (blue circles) and 600 nm (purple triangles). (b) Blue squares are for the plot of a/λ at the wavelength with the 20% transmission for the transmission dip for the periods of 350, 500 and 765 nm, respectively, for the on-resonance case. The purple triangles show transmission dip width at 40% for the off-resonance case. The thickness of the GPSC is 400 nm.

When the GPSC thickness D is near the values of the coupled equations $a/\lambda = \{0.41, 0.49\}$ and $\lambda = n \times D$, off-resonance conditions exist. The purple triangles in Fig. 4(a) show a transmission through the GPSC for the parameters a = 765 nm and D = 600 nm (off-resonance thickness). The average of the minimum of the transmission dip is around 20%, 10% higher than that in the on-resonance case. In addition to the shallow dip in transmission in the off-resonance case, the width is much narrower than that for the on-resonance case. Next, the thickness of the GPSC was fixed at 400 nm (off-resonance thickness) for periods of 350, 500 and 765 nm and computed the transmission through the GPSC. The width (at 40%) of transmission dip became smaller from a width of 422, 204, to 78 nm for periods of 765, 500 and 350 nm, respectively as shown in purple triangles in Fig. 4(b). There is 75% transmission through GPSC with a thickness of 400 nm and a period of 350 nm even when the light is in the photonic band gap of the graded region, for the off-resonance case.

Fig. 5 shows transmission spectra for the GPSC with a unit cell size of $18a \times 18a$ (a=350 nm) and a slab thickness of 242 nm. For one transmission simulation, the material in GPSC has a real dielectric constant of 12 (red circles). The real and imaginary refractive indexes of silicon [36] were used in the simulation for the other transmission in the figure (blue squares). The transmission dip location is red-shifted as the real refractive index in silicon in near-infrared is higher than the square root of 12 [36]. By including the imaginary part of the refractive index, the transmission dips near 540 nm and between 760 and 860 nm are closer to 0% comparatively

to the transmission with only the real refractive index. In this case, the light coupling between in-plane and out-of-plane resonances is still effective in the GPSC with absorbing materials.

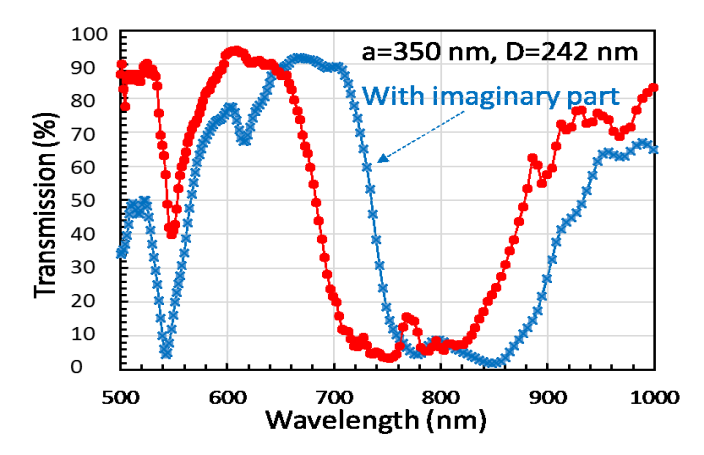


Figure 5. Transmission of normal incident light through the GPSC with a unit cell size of 18a×18a (a=350 nm) and a slab thickness of 242 nm with a dielectric constant of 12 (red circles) and with real and imaginary refractive index (blue squares).

5. Conclusions

In summary, cavities in GPSCs have been observed in the simulation due to the dislocation of photonic band gaps in the side graded regions and the central near-uniform region. Cavities can be formed in the 8 side graded regions, the central region or the boundary between graded and uniform regions. The boundary cavity mode can have a high Q-factor of up to 5.8×10^5 . The central cavity resonance extends over multiple unit cells. Thus, it has a small Q-factor, radiates in out-of-plane direction and couples with out-of-plane resonance. Broadband, deep transmission dips have been observed in the on-resonance case at the locations of the photonic band gaps for the graded regions, indicating the coupling of in-plane central cavity resonances with the F-P resonance in GPSC. When the thickness of the GPSC is out-of-resonance with the central cavity mode, the transmission is high even when the light in the photonic band gap range.

Funding

National Science Foundation (NSF) (1661842 and 1661749).

References

- John D. Joannopoulos, Steven G. Johnson, Joshua N. Winn & Robert D. Meade, Photonic Crystals: Molding the Flow of Light (second edition) (Princeton University Press).
- T. Asano, B. S. Song, and S. Noda, "Analysis of the experimental Q factors (~ 1 million) of photonic crystal nanocavities," Opt. Express 14, 1996–2002 (2006).
- Y. Akahane, T. Asano, B. S. Song, and S. Noda, "High-Q photonic nanocavity in a two-dimensional photonic crystal," Nature 425, 944

 –947 (2003).
- Aniwat Tandaechanurat, Satomi Ishida, Denis Guimard, Masahiro Nomura, Satoshi Iwamoto and Yasuhiko Arakawa, "Lasing oscillation in a three-dimensional photonic crystal nanocavity with a complete bandgap," Nat. Photonics 5, 91-94 (2011).
- M. Qi, E. Lidorikis, P.T. Rakich, S.G. Johnson, J.D. Joannopoulos, E.P. Ippen, and H.I. Smith, A threedimensional optical photonic crystal with designed point defects. Nature 429, 538-542 (2004).
- O. Painter, R. K. Lee, A. Scherer, A. Yariv, J. D. O'Brien, P. D. Dapkus, and I. Kim, "Two-dimensional photonic band-gap defect mode laser," Science 284, 1819-1821 (1999).
- M. Loncar, T. Yoshie, A. Scherer, P. Gogna, and Y. Qiu, "Low-threshold photonic crystal laser", Appl. Phys. Lett. 81, 2680-2682 (2002).
- Sanfeng Wu, Sonia Buckley, John R. Schaibley, Liefeng Feng, Jiaqiang Yan, David G. Mandrus, Fariba Hatami, Wang Yao, Jelena Vuckovic, Arka Majumdar9 & Xiaodong Xu, "Monolayer semiconductor nanocavity lasers with ultralow thresholds," Nature 520, 69 (2015).

- J. D. Joannopoulos, P.R. Villeneuve, and S.H. Fan, Photonic crystals: putting a new twist on light. Nature 386, 143-149 (1997).
- S. H. Kim, H. Y. Ryu, H. G. Park, G. H. Kim, Y. S. Choi, Y. H. Lee, and J. S. Kim, "Two-dimensional photonic crystal hexagonal waveguide ring laser," Appl. Phys. Lett. 81, 2499-2501 (2002).
- H. Altug and J. Vuckovic, "Two-dimensional coupled photonic crystal resonator arrays," Appl. Phys. Lett. 84, 161-163 (2004).
- Shanhui Fan, Pierre R. Villeneuve, J. D. Joannopoulos, and H. A. Haus, "Channel Drop Tunneling through Localized States," Phys. Rev. Lett. 80, 960 (1998).
- 13. S.-H. Kwon, S.-H. Kim, S.-K. Kim, Y.-H. Lee, and S.-B. Kim, "Small, low-loss heterogeneous photonic bandedge laser," Opt. Express 12, 5356 (2004).
- F. Bordas, M. Steel, C. Seassal, and A. Rahmani, "Confinement of band-edge modes in a photonic crystal slab," Opt. Express 15, 10890 (2007).
- 15. L. Ferrier, P. Rojo-Romeo, E. Drouard, X. Letartre, and P. Viktorovitch, "Slow Bloch mode confinement in 2D photonic crystals for surface operating devices," Opt. Express 16, 3136 (2008).
- P. Nedel, X. Letartre, C. Seassal, A. Auffe'ves, L. Ferrier, E. Drouard, A. Rahmani, and P. Viktorovitch, "Design and investigation of surface addressable photonic crystal cavity confined band edge modes for quantum photonic devices." Opt. Express 19, 5014 (2011).
- 17. A. V. Giannopoulos, Y.-J. Li, C. M. Long, J.-M. Jin, and K. D. Choquette, "Optical properties of photonic crystal heterostructure cavity lasers," Opt. Express 17, 5379 (2009).
- Xiaochen Ge, Momchil Minkov, Shanhui Fan, Xiuling Li, and Weidong Zhou, "Low index contrast heterostructure photonic crystal cavities with high quality factors and vertical radiation coupling," Appl. Phys. Lett. 112, 141105 (2018).
- D. Lowell, J. Lutkenhaus, D. George, U. Philipose, B. Chen, and Y. Lin, "Simultaneous direct holographic fabrication of photonic cavity and graded photonic lattice with dual periodicity, dual basis, and dual symmetry," Opt. Express 25, 14444 (2017).
- David Lowell, Safaa Hassan, Oliver sale, Murthada Adewole, Noah Hurley, Usha Philipose, Banglin Chen and Yuankun Lin "Holographic fabrication of graded photonic super-quasi-crystal with multiple level gradients", Applied Optics 57, 6598 (2018).
- David Lowell, Safaa Hassan, Murthada Adewole, Usha Philipose, Banglin Chen and Yuankun Lin, "Holographic fabrication of graded photonic super-crystals using an integrated spatial light modulator and reflective optical element laser projection system," Appl. Opt. 56, 9888 (2017).
- 22. Safaa Hassan, Oliver Sale, David Lowell, Noah Hurley, and Yuankun Lin, "Holographic fabrication and optical property of graded photonic super-crystals with a rectangular unit super-cell," Photonics 5, 34 (2018).
- Safaa Hassan, David Lowell, and Yuankun Lin, "High light extraction efficiency in organic light-emitting diodes by patterning the cathode in graded superlattice with dual periodicity and dual basis," J. Appl. Phys. 121, 233104 (2017).
- C. Smith, H. Benisty, D. Labilloy, U. Oesterle, R. Houdré, R. De La Rue, C. Weisbuch, "Near-infrared microcavities confined by two dimensional photonic bandgap crystals," Elec. Lett. 35, 228 (1999).
- M. Bandres, S. Wittek, G. Harari, M. Parto, J. Ren, M. Segev, D. Christodoulides, M. Khajavikha, "Topological insulator laser: Experiments," Science 359, eaar4005 (2018).
- 26. Oliver Sale, Safaa Hassan, Noah Hurley, Khadijah Alnasser, Usha Philipose, Hualiang Zhang, and Yuankun Lin, "Holographic fabrication of octagon graded photonic super-crystal and potential applications in topological photonics," Frontiers of Optoelectronics (2019). https://doi.org/10.1007/s12200-019-0941-2
- C. Hsu, B. Zhen, A. Stone, J. Joannopoulos, M. Soljačić, "Bound states in the continuum," Nature Reviews Materials 1, 16048 (2016).
- 28. Joshua Hendrickson, Junpeng Guo, Boyang Zhang, Walter Buchwald, and Richard Soref, "Wideband perfect light absorber at midwave infrared using multiplexed metal structures," Opt. Lett. 37, 371-373 (2012).
- Chenggang Hu, Liyuan Liu, Zeyu Zhao, Xu'nan Chen, and Xiangang Luo, "Mixed plasmons coupling for expanding the bandwidth of near-perfect absorption at visible frequencies," Opt. Express 17, 16745-16749 (2009).
- S. Johnson and J. Joannopoulos, "Block-iterative frequency-domain methods for Maxwell's equations in a planewave basis," Opt. Express. 8, 173–190 (2001).
- V.A. Mandelshtam and H.S. Taylor, "Harmonic inversion of time signals," J. Chem. Phys. 107, 6756

 –6769
 (1997).
- 32. A.F. Oskooi, D. Roundy, M. Ibanescu, P. Bermel, J.D. Joannopoulos and S.G. Johnson, "MEEP: a flexible free-software package for electromagnetic simulations by the FDTD method," Comput. Phys. Commun. 181, 687–702 (2010).
- S. Hassan, K. Alnasser and Y. Lin, "Effects of Photonic Band Structure and Unit Super-Cell Size in Graded Photonic Super-Crystal on Broadband Light Absorption in Silicon," Photonics 6, 50 (2019).
- W. Zhou, S. Liu, X. Ge, D. Zhao, H. Yang, C. Reuterskiöld-Hedlund and M. Hammar, "On-Chip Photonic Crystal Surface-Emitting Membrane Lasers (Invited)," IEEE Journal of Selected Topics in Quantum Electronics 25, 4900211 (2019).
- 35. W. Zhou, D. Zhao, Y. Shuai, H. Yang, S. Chuwongin, A. Chadha, J. Seo, K. Wang, L. Liu, Z. Ma, S. Fan, "Progress in 2D photonic crystal Fano resonance photonics," Progress in Quantum Electronics 38, 1–74 (2014).

36.	M. Green, "Self-consistent optical parameters of intrinsic silicon at 300 K including temperature coefficients," Solar Energy Materials & Solar Cells 92 , 1305–1310 (2008).